Using Focused Acoustic Excitation to Accelerate Crack Healing

Brian C. Fehrman* Eric A. Petersen† Katherine A. Barnes‡ and Umesh A. Korde§

This paper presents recent investigations on an approach to accelerate the natural healing processes occurring in a polymer aggregate. In a space structure where the processes leading to healing must continuously compete with the mechanisms producing structural damage (such as micrometeor strikes), methods aimed at accelerating healing could prove valuable. The technique examined here is based on the use of focused acoustic energy to influence the crack healing dynamics via increased pressure and temperature at the crack site. No knowledge or interference of crack location are required with this approach. Here we present our recent results on a study of epoxy curing as an analog to the healing process, and in particular, present in detail our experimental application of time reversed acoustics to focus longitudinally propagating pulses and chirp signals in metal rods. Extensions to other media are in progress.

Nomenclature

R = Recovery Ratio
E_∞ = Fracture Energy
σ_∞ = Fracture Stress
γ = Tensile Modulus
D_c = Reptation Diffusion Coefficient

I. Introduction

There are many instances when minor damage affects the functionality of difficult to access space structures. Often the damage is caused by collisions with space debris and is nearly impossible to repair when employing the traditional method of reaching the damaged site manually. It is therefore important to consider materials and structures with built-in mechanisms for self-repair.[1] Research on self-healing materials has seen a rapid growth in recent years, though the emphasis thus far appears to have been on developments, including increasing the rate of recovery, at the materials level.[2–8] Many applications have relied on heating/cooling to both initiate and speed the recovery process.[9–14] Some research has also been done on the effect of introducing ultra-violet light during the recovery stage.[15] The rate of healing is crucial from a structural point of view, given that the healing process frequently must compete with the damage-inducing processes in an application. Our study considers the problem from a structural point of view, while recognizing that healing occurs at the molecular/materials-level. In particular, the current emphasis is on investigating whether crack healing to the point of full mechanical recovery can be accelerated using focused acoustic energy.

An appealing method for focusing energy at a damaged point is one that realizes a defect has occurred, but does not need actual knowledge of where that defect is located. One method that has been investigated

*Advanced Dynamics Laboratory, Research Assistant, Department of Computer Science, 501 E. St. Joseph Street, Rapid City, SD 57701, AIAA Student Member.
†Advanced Dynamics Laboratory and Research Assistant, Department of Physics and Astronomy, University of Nebraska-Lincoln, Lincoln, NE 68504, AIAA Student Member.
‡Advanced Dynamics Laboratory, Research Assistant, Department of Interdisciplinary Sciences, 501 E. St. Joseph Street, Rapid City, SD 57701, AIAA Student Member.
§Professor, Mechanical Engineering Department, 501 E. St. Joseph Street, Rapid City, SD 57701, AIAA Member

is the time-reversal method. There are many different applications and methods of time-reversal that have been researched.[16–20] One particular method of time-reversal involves an emitting source and receiving sources. The emitter sends a signal through a medium and the receivers record that signal. If a defect is present, it will affect the way in which the signal travels through the medium. This provides a way to detect if damage has occurred and to begin focusing acoustic energy at that point without actually knowing where the defect is. If the receivers time reverse and play back the signals they read in, those played back signals will combine together and focus on the damage point. Our work is based on the use of this technique for the purpose of focusing acoustic energy at a damage point in order to accelerate the recovery rate of the self-healing material at that point.[16,21]

A. Theory

Based on Wool and O'Connor (1981),[21] crack healing in polymers proceeds in the following stages: (i) surface rearrangement, (ii) surface approach, (iii) wetting, (iv) diffusion, and (v) equilibrium and randomization. During healing, the "recovery ratio," R, defined as the rate of recovery of mechanical properties (e.g. tensile modules, fractile stress, etc.) depends, among other factors, on the molecular weight, time, temperature and pressure. An acoustic/stress wave propagating through a structure represents a propagating stress field that may be highly localized depending on the shape and value of the propagating wave form. A localized stress field at a crack could thus lead to an increase (or decrease) in the pressure and temperature at the crack. Therefore, in theory, a highly localized focused pulse at a crack could have a significant impact on the healing rate.

Calculations were carried out based on the Wool and O'Connor theory to determine (i) the optimal shape of a pulse to be focused at a crack, and (ii) the effect of the pulse "magnitude" on the recovery ratio, R.

For cracks with small, smooth surface areas, the recovery rate R can be estimated using

$$R = R_0 + \frac{kt^{1/4}}{\sigma_\infty} \tag{1}$$

Where

$$R_0 = \frac{{\sigma_0}^2}{2\gamma E_\infty} \quad \text{and} \quad K = \frac{qn_0}{(2D_c)^{1/4}} \tag{2}$$

where E_∞, σ_∞, and γ are the fracture energy, fracture stress and tensile modulus respectively.

The acoustic stress-wave pulse is here taken to determine the stress σ_0 associated with wetting and surface attraction. D_c is the reptation diffusion coefficient, n_0 is related to the bulk density, molecular weight, Avogadro's number, etc. The parameter q relates the stress due to interpenetration normal to the surface to the number of constraints in the interpenetration volume. Figure 1 shows the effect of pulse height (directly related to the extent of focusing and the initial pulse height) on the recovery ratio. The recovery ratio is affected by the pulse in the early stages of healing and greater pulse heights for the given width are seen to improve the recovery rate in the earlier stages.

II. Experimental Implications

Our studies so far have sought to answer two essential questions: (1) the effect of acoustic excitation on the healing process, and (ii) the focusing of acoustic pulses at a defect. To facilitate investigations on the first question, we study polymer curing as a controlled, repeatable analog of the healing process. For acoustic focusing, we use the time-reversal technique developed by Fink et al. (1995), and test it in a 1-dimensional context using extensional wave pulses. Details on these tests are discussed below.

A. Epoxy Curing Studies

For the epoxy curing studies, the epoxy resin Huntsman GY 6010 (composed primarily of Bisphenol A) and the hardener Huntsman HY 955 were mixed 100 parts to 35 parts, respectively, by weight. It may be of particular note that HY 955 is an amide rather than an amine. Hardening components in two part epoxy are almost always amines; however, amides boast superior chemical bond stability and do not have as many difficulties curing in the presence of humidity.

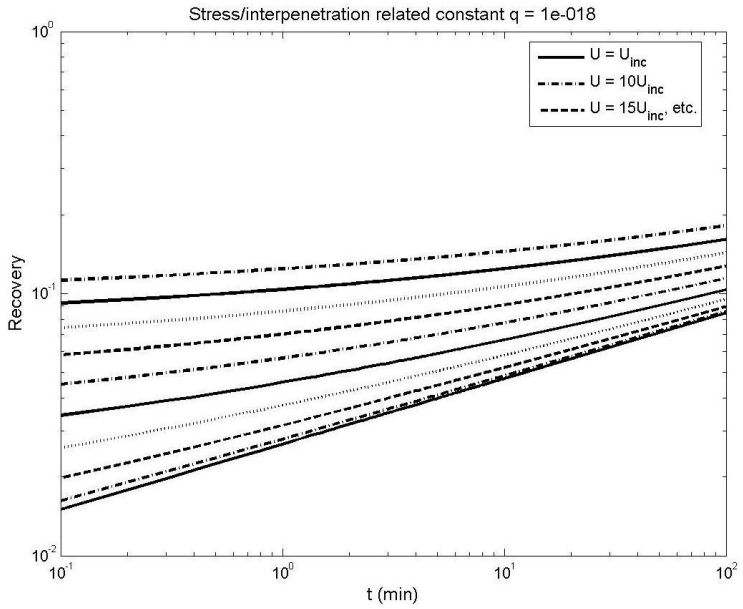

Figure 1. Effect of pulse height on recovery rate at $q = 1^{-18}$. Note the scale on the vertical axis.

A brass tube of half-inch diameter is filled with fully mixed epoxy and monitored during the curing process. The brass tube has a calculated natural frequency of 100 kHz. Using a piezo-ceramic transducer, an artificial waveform generator (AWG) feeds signals to the tube from 95–115 kHz. Signals are fed at one end of the tube and received at the other with a piezo-ceramic transducer.

Throughout the testing process, epoxy has been monitored for the full twenty-four hour cure time, six hour, and three hour tests. All of these tests allow the epoxy the full hour of set time, plus additional time to monitor the cure process. All tests show the cured epoxy produces significantly more defined wave patterns.

Additionally, because the test results showed such significant difference between cured and uncured epoxy, it was thought air bubbles may be interfering with the coupling of the transducer to the tube. To prevent this problem in the future, the epoxy was degassed under vacuum for ten minutes, at twenty-five inches of mercury, and then allowed to stand for ten minutes. This process significantly reduced the amount of air bubbles in the mixture.

The fully cured and empty brass tubes were characterized with impact testing. The focus here has been verifying our previous results on acoustic monitoring of the epoxy curing process. In particular, it was considered important to verify that the frequency response function for the tube with the fully cured epoxy was significantly different from that for the empty tube. The frequency response functions for both situations were obtained by taking the Fourier transform of the impulse response. Each test was run three times to ensure repeatability.

B. Computerized Testing

Two separate test methods were implemented for the computerized testing. These tests were performed in order to prove that we can perform the time-reversal portion of the project that is needed for the self-healing.

1. Computerized Time Reversal Test Method 1

The first experimental work performed for the time-reversal portion of the self-healing involved the setup of a one-dimensional acoustic wave transmission scenario constructed on a vibration-canceling optics table (Figure 4). The medium used for the waves to propagate through was a steel rod measuring 0.3048 m in length and 19.05 mm in diameter. Three piezo-ceramic stacks (PZTs) measuring 11.2 mm thick and 13.4 mm in diameter were used in the experiment. Two of the PZTs (PZT0 and PZT1) acted as transducers in which they were both a receiver and an actuator. These two PZTs were attached to each end of the steel rod using

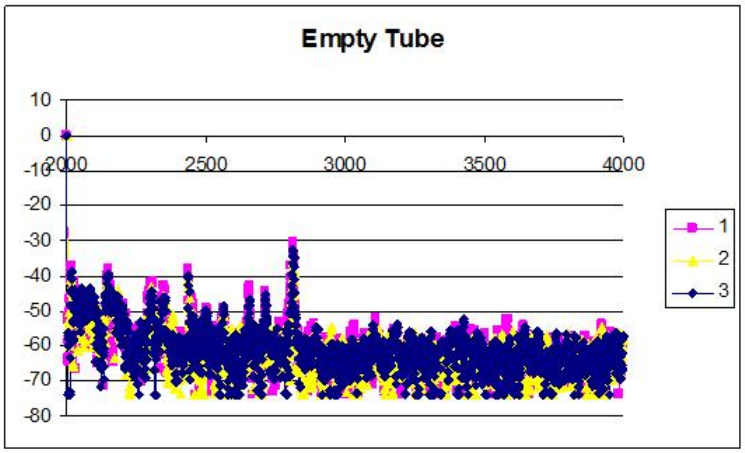

Figure 2. Frequency response function for the empty tube (dB on the vertical axis).

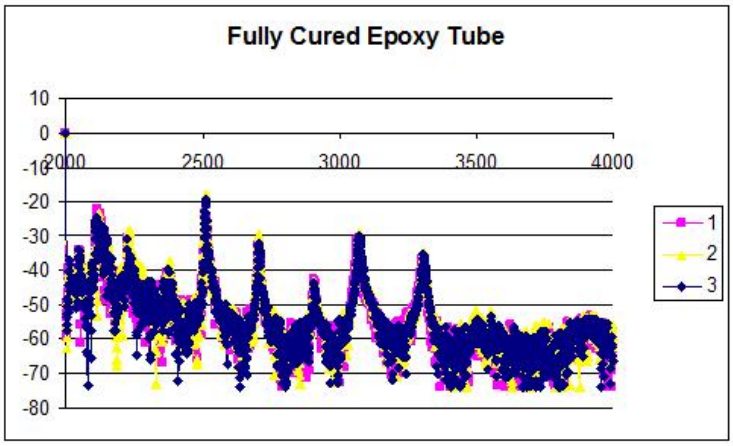

Figure 3. Frequency response function for the tube with fully cured epoxy (dB on the vertical axis).

accelerometer putty. The third PZT (PZT2) acted solely as a receiver and was attached behind one of the transducer PZTs (PZT1) also using accelerometer putty (5). The rod with the PZTs on each end was then tensioned between two high-power, switchable magnetic bases.

A computer-controlled, multi-functional data acquisition (DAQ) card with an onboard field programmable gate array (FGPA) chip installed in a PXI chassis using an external input/output board was used for the sending, acquiring, and processing of the acoustic wave signals. The FPGA card possesses an analog sampling speed of 768 kHz and an analog output speed of 1.0 MHz with ±2.5 mA of current. The IO board was fitted with five BNC cables; two for handling the input and the output for PZT0 (Channel 0), two for handling the input and output for PZT1 (Channel 1), and one to handle the input for PZT2 (Channel 2). For each PZT, a 1.0 MΩ resistor had been placed in parallel across the wires in order to make the current produced by the stacks readable by the DAQ card.

Software was written that set up a single 100 kHz sinusoidal pulse with 20 V of peak-to-peak amplitude. This pulse was then played out by PZT0. Immediately after the pulse was sent, the program began recording from PZT0 and PZT1 until 25,000 samples were read in from each PZT. This data was then sent back to the desktop computer so that the signals received from each PZT could be saved and manipulated. Several different combinations of data manipulation were performed, including: not doing anything with the signals, reversing both of the signals, reversing only the signal from PZT0, reversing only the signal from PZT1, reversing both signals and phase shifting the signal from PZT0 by 180°, reversing both signals and phase

shifting the signal from PZT1 180°, and reversing both signals then phase shifting both 180°. The data was then normalized and multiplied by 10 to give a maximum amplitude of 20 V peak-to-peak again. These signals were then sent back to the DAQ card. After receiving the manipulated signals from the desktop, the DAQ card then played back the signals through their respective PZTs continuously while at the same time recording at PZT2 (the "defect" PZT that sits behind PZT1). The maximum peak-to-peak amplitude read in from PZT2 during the playback was continuously updated and displayed.

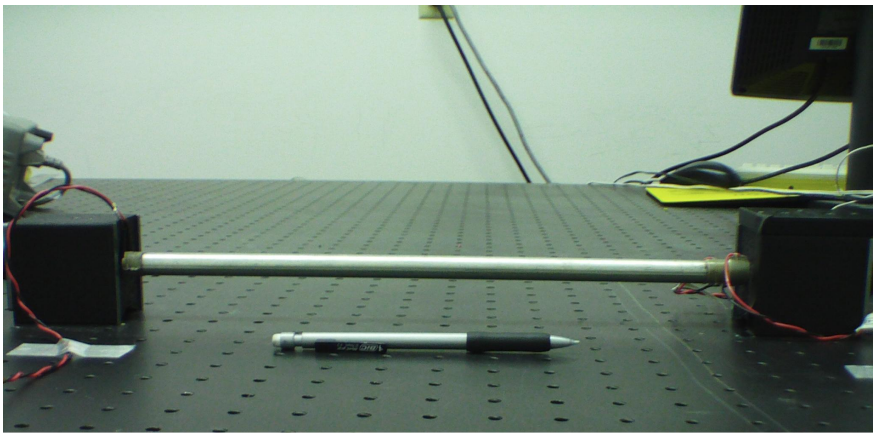

Figure 4. One-dimensional time-reversal setup on an optics table.

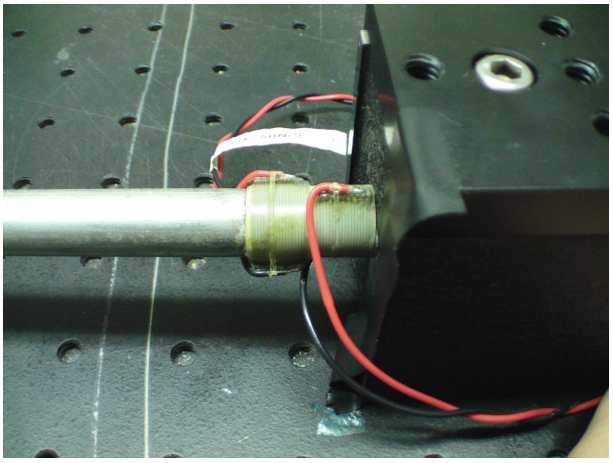

Figure 5. PZT2 (right), the "defect" PZT, is placed behind PZT1 (left).

2. Computerized Time Reversal Test Method 2

The setup for Test Method 2 is somewhat similar to the setup for Test Method 1. This setup also used the vibration-canceling optics table and was a one-dimensional acoustic wave transmission scenario. A steel rod with the same diameter and material of the rod from Test Method 1 was used. This rod, however, was 0.6096 m in length (twice the length of the rod from Test Method 1). A custom tensioning system was constructed to be used in place of the switchable magnetic bases. This system allowed for a more constant pressure than the magnetic bases. A thin piece of styrofoam cushion was placed underneath of the rod in order to keep it from touching the optics table. The "defect" PZT that was used in Test Method 1 has now been taken out of this setup. The algorithm used for Test Method 2 is different than the one for Test Method 1. Because of this, we are looking at the focusing a little differently and do not require the "defect" PZT in that location for this test. Figures 6, 7 and 8 show pictures of the current setup to clarify what it is.

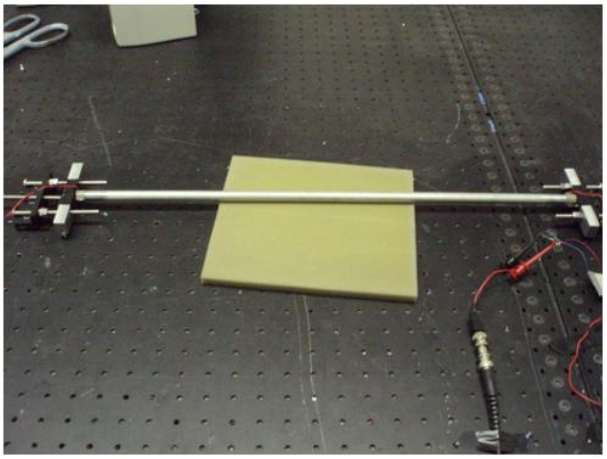

Figure 6. Overview of setup for Time Reversal Test Method 2.

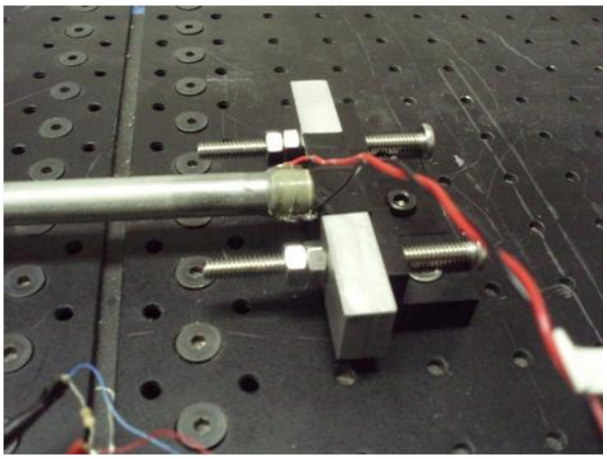

Figure 7. Close-up of PZT1.

The National Instruments 7853R FPGA DAQ card that we are currently using is capable of outputting a maximum power of 20 V peak-to-peak. Although this is a sufficient voltage to drive the piezoelectric ceramic stacks, the current that it outputs is only 2.5 mA. This small a current was able to lightly excite the PZTs and produce a readable signal through the shorter steel rod, but not at an amplitude that would be useful for our future testing. For these reasons, we made the decision to create a custom-built, multi-channel, voltage/current amplifier that is capable of providing an amplification of ~ 30 V peak-to-peak and a current of up to ~ 2.0 A (Figure 9).

The algorithm that is used for this test setup is as follows:

1. PZT0 sends a Multi-Tone Pulse (a "chirp") through the rod and towards PZT1.
2. PZT0 and PZT1 read in 1000 samples.
3. Using normalized correlation, the signal read by PZT0 is searched for the reflection of the pulse that was sent out. This reflection pulse will be the original pulse with a 180° phase shift.
4. The amplitude of this reflection pulse is recorded, along with the index in the signal that corresponds to the beginning of this pulse (i.e., the position where the reflection pulse was found).
5. This pulse is extracted, centered on zero and then re-scaled to be maximum amplitude.

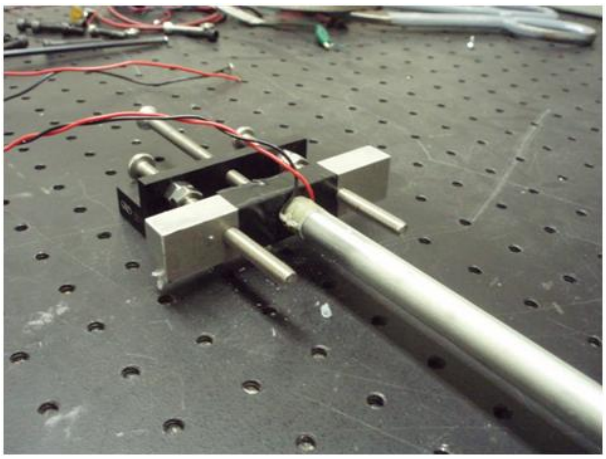

Figure 8. Close-up of PZT0.

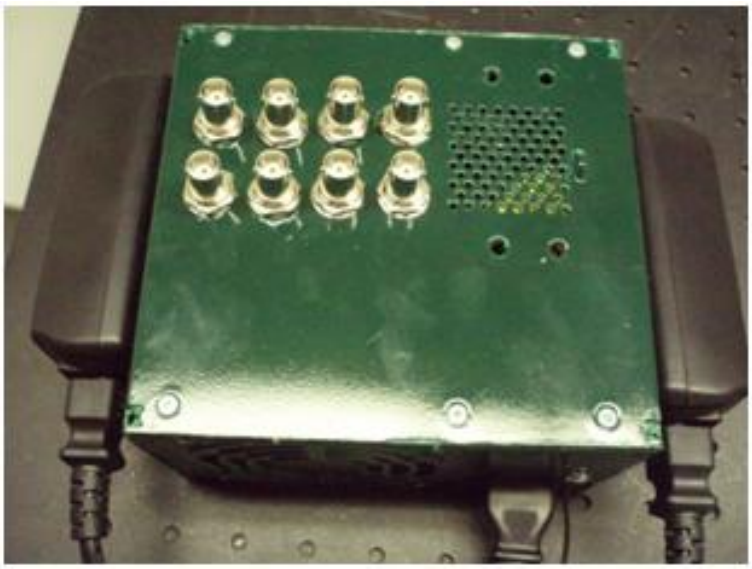

Figure 9. Top-view of amplifier.

6. Steps 3-5 are performed on the signal read by PZT1, except it will just be looking for the original pulse that was sent by PZT0.
7. After obtaining the indices for the position of where each pulse was found, and also the pulse itself, all of the other information in the signals is zeroed out. This means the signals that were read by each PZT will now only contain the pulses found. These pulses have been centered on zero and re-scaled to maximum amplitude as a result of Step 5.
8. These modified signals are then completely reversed.
9. These reversed signals are then played back by the corresponding PZT that originally read them in.
10. PZT0 and PZT1 then read 1000 samples.
11. The signal from PZT0 is then parsed to try to find the reflection pulse. This process uses the normalized correlation again.

12. Once the reflected pulse is found (the original pulse shifted 180°), its amplitude is recorded and compared to the amplitude from the reflection pulse obtained from Step 4 that was performed on PZT0.

Essentially what is happening is that PZT0 sends its pulse. PZT1 records this pulse. The pulse hits PZT1 and reflects back to PZT0 with a 180° phase shift. PZT0 records this reflection. During playback, PZT0 will play back the reversed reflection that it read in. This will travel towards PZT1. At the time it reaches PZT1 and begins reflecting again is when PZT1 will begin to play out the reversed original pulse that it had read in. These two pulses (the one sent by PZT0 and the one being played out by PZT1) will combine together and travel back towards PZT0. This causes PZT0 to receive the combined amplitudes of the reflection pulse and the pulse played out by PZT1. This is greater amplitude than could be achieved by either pulse alone.

For this testing setup we switched to using a multi-tone pulse instead of a single-tone pulse because we not only get better excitation, but we are also more easily able to find this pulse in the signals that are read in by each PZT.[20] We switched to using a longer rod in order to accommodate this longer pulse. The pulse we are using consists of a 130 kHz pulse in the center, a 110 kHz pulse on both sides of it, and then a 90 kHz pulse to the outside of each of the 110 kHz pulses. These are strung together to form a single, multi-tone pulse. You can see the additional "defect" PZT is not needed for these particular tests because we are proving focusing at PZT0, the original sending PZT itself.

C. Results

In order to have a properly functioning crack healing system, there must be two working components: a computer driven test system to send signals and detect the crack and a system of material which has been characterized. In this study, we have utilized computerized testing and epoxy curing studies as separate experiments. This paper focuses more heavily on the time-reversal portion of the system and will only go over those results.

1. Computerized Time Reversal Test Method 1 Results

Figure 10 displays the initial 100 kHz pulse that is set up and sent out by PZT0. Figure 11 shows that the initial pulse that is received by PZT1 is very close to the same pulse that is sent from the transducer PZT0. Calculations performed involving the number of data points read in and the sampling speed of the DAQ card showed that the times at which the initial pulse and first reflection were received are consistent with the speed of an acoustic wave propagating through a steel rod. This further confirmed that what is seen is actually what was sent out and reflected back. Each of the test combinations mentioned in the previous section was run five times and the mean of each of their data sets were compared (Table 1). The highest average peak-to-peak amplitude was achieved with reversing both signals and phase shifting the signal read by PZT0 180°. Very close to that was the amplitude that was reached by reversing both signals and phase shifting the signal read by PZT1 180°. As can be seen in Table 1, both of these combinations are significantly higher amplitudes than the other combinations. This suggests that the time-reversal may be causing a focusing of the waves at the reflection point.

Combination	**Average Max PPV**
Not Reversed	0.843750
Both Reversed	0.918213
Only PZT0 Signal Reversed	0.790344
Only PZT1 Signal Reversed	0.846252
Both Reversed, PZT0 Signal Phase Shifted 180 Degrees	1.014770
Both Reversed, PZT1 Signal Phase Shifted 180 Degrees	1.009700
Both Reversed, Both Phase Shifted 180 Degrees	0.908142

Table 1. Chart showing the average maximum peak-to-peak amplitude for each experimental combination that was performed.

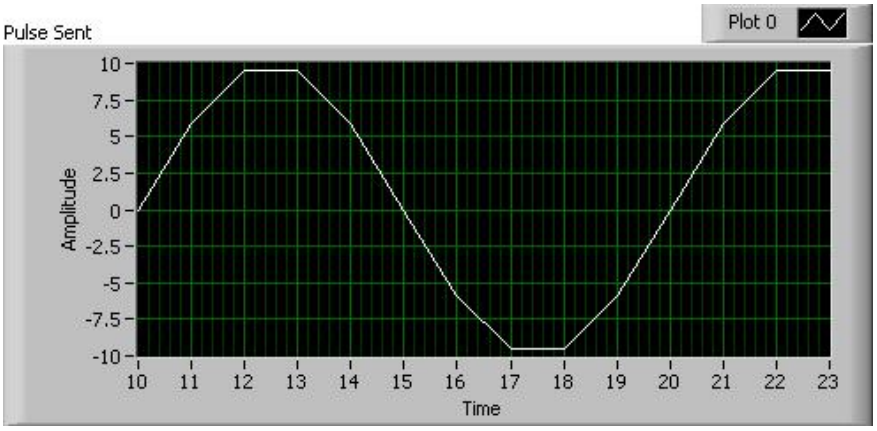

Figure 10. Initial 100 kHz pulse sent by PZT0.

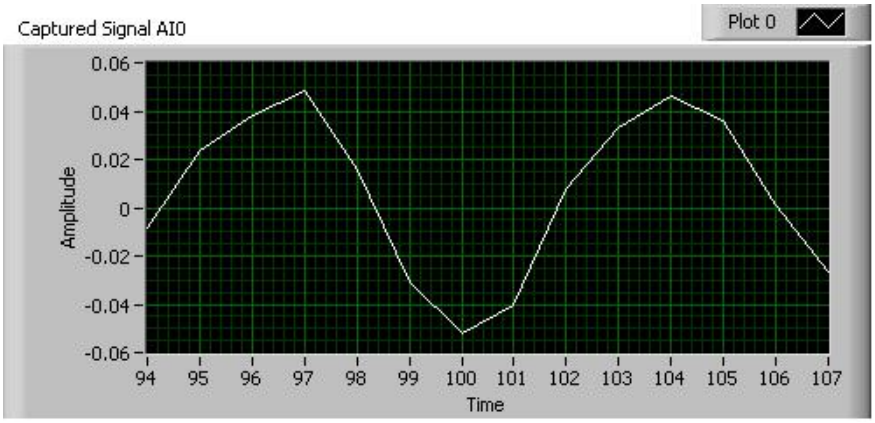

Figure 11. First pulse received by PZT1.

2. Computerized Time Reversal Test Method 2 Results

Figure 12 shows the initial multi-tone pulse that is sent by PZT0 towards PZT1. This is what the algorithm searches for in the signal read by PZT1. The reflection pulse that is received by PZT0 is just the pulse that is initially sent phase shifted by 180°; this is shown in Figure 13. This is what the algorithm searches for in the signal read by PZT0. Figures 14 and 15 show the first 400 samples that are read by their respective PZTs after the initial pulse is sent by PZT0. You can see in Figure 14 that the initial pulse starts to appear at the 82nd sample read in by PZT1. In Figure 15, you can see that the reflected pulse begins to appear at the 164th sample read in by PZT0; this is exactly twice the amount of time it took for the pulse to travel from one end of the rod to the other. These times (82nd and 164th sample) were consistent through every test performed with this system. Figures 16 and 17 show what is played back by each PZT during the reversal portion of the algorithm. These played-back signals contain the extracted pulses (regular pulse for PZT1 and reflected pulse for PZT0) at their correct time locations relevant to one another and with all other data zeroed out. Figure 18 shows the signal that is read by PZT0 during the reversal phase. Compare this to the signal read by PZT0 during that initial phase (Figure 15). The signal read during the reversal phase not only has greater amplitude, but is also much more defined.

Table 2 shows the amplitude of the reflection pulse recorded at PZT0. Notice that the reversal reflection amplitude is more than double the amplitude of the initial reflection pulse recorded. Another item to note is that if you sum the amplitudes recorded for the single channel playbacks (one PZT plays back a signal while the other plays out 0V) it is close to equaling the amplitude that is achieved when both channels are

used during the time-reversal. This supports that the pulses are combining during the time-reversal. Also notice that when PZT0 alone plays back during the time-reversal portion, the reflection it receives is stronger than the reflection received in the initial pulse sending (Step 2). This is consistent with another form of the time-reversal known as the iterative time-reversal process.[16]

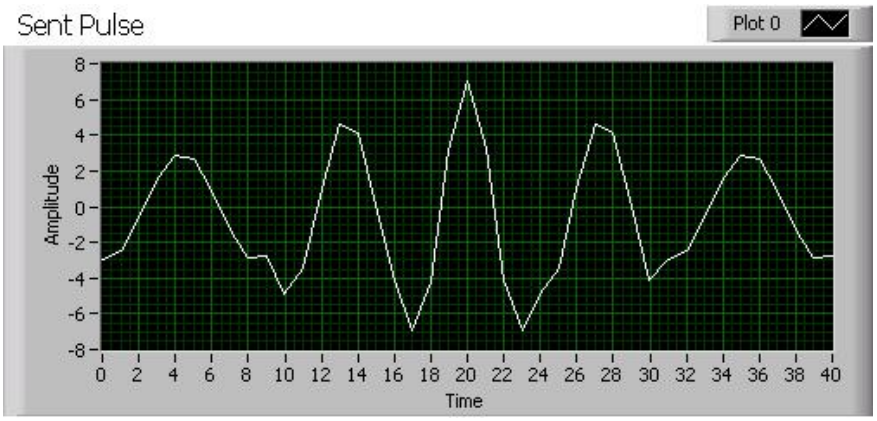

Figure 12. Initial multi-tone pulse sent by PZT0.

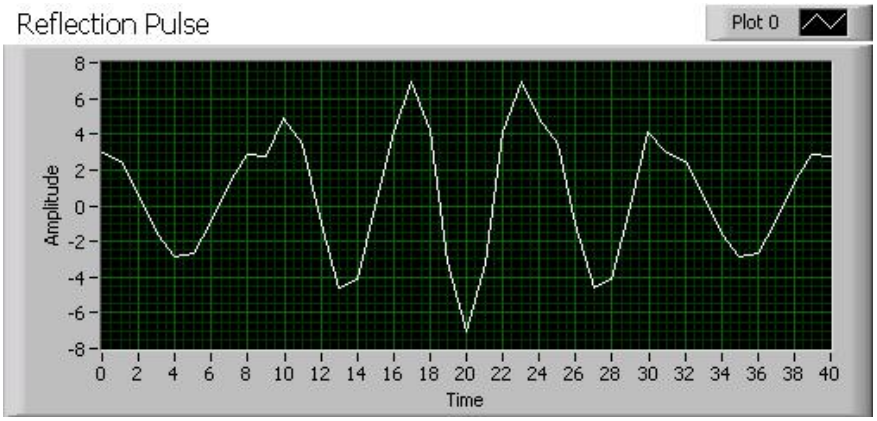

Figure 13. Reflection of the multi-tone pulse.

PZT0 Initial Reflection Amplitude	147.135 mV
PZT0 Reversal Reflection Amplitude	333.374 mV
PZT0 Reversal Reflection Amplitude with only PZT1 replaying a signal	194.213 mV
PZT0 Reversal Reflection Amplitude with only PZT0 replaying a signal	173.584 mV

Table 2. Chart showing the average maximum peak to peak amplitudes recorded during the experiments for Test Method 2.

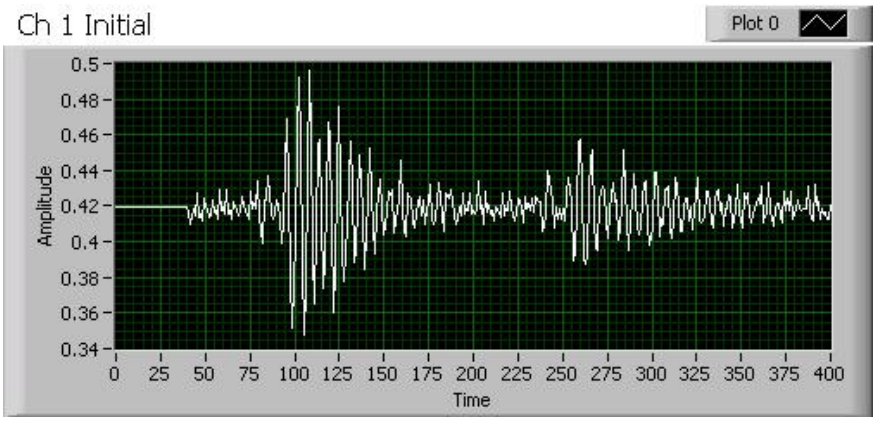

Figure 14. Recording from PZT1 during step 2. The initial pulse starts to appear at the 82nd sample.

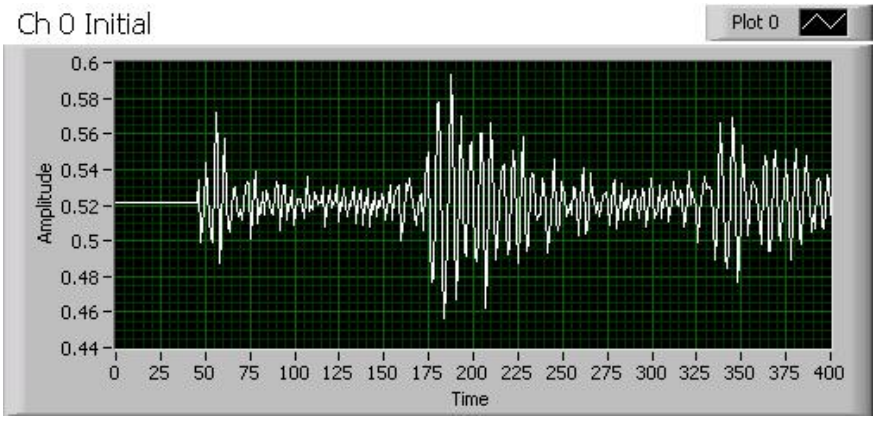

Figure 15. Recording from PZT0 during step 2. The reflected pulse starts to appear at the 164th sample.

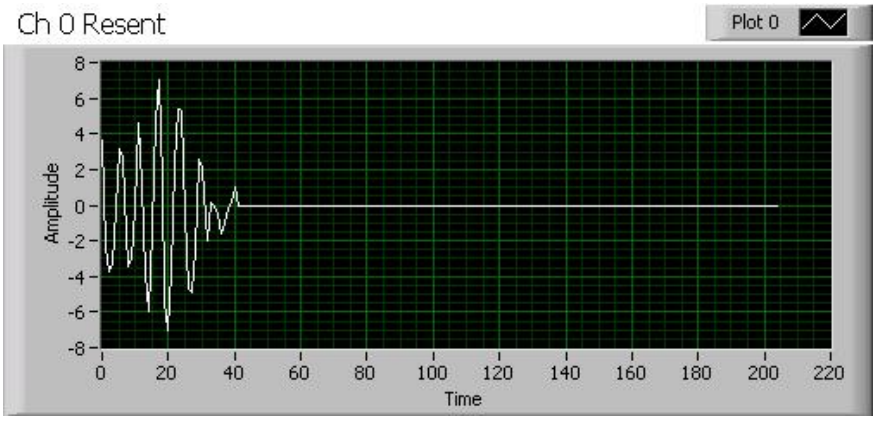

Figure 16. Signal that is played out by PZT0 during step 9. It is the rescaled, centered and reversed reflection pulse that was received. Since this was read last, it will be played back first. Everything else is zeroed out.

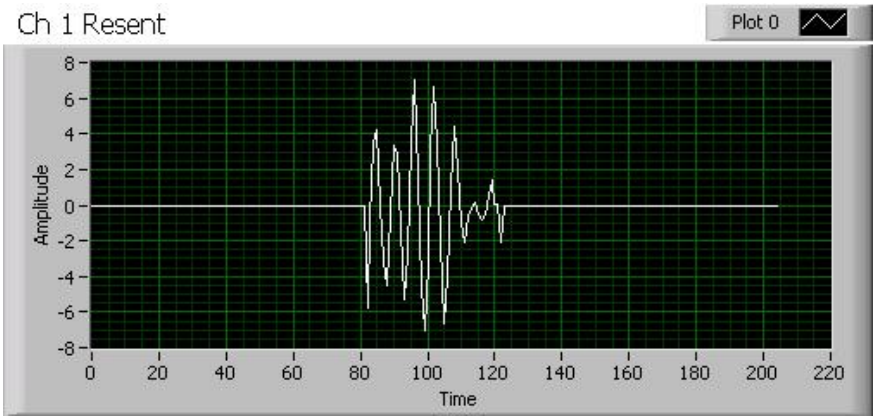

Figure 17. Signal that is played out by PZT1 during step 9. It is the rescaled, centered and reversed initial pulse that was received. Since this was read first, it will be sent out last. The data in front and behind of the pulse are zeroed out. Remember that it takes approximately 82 time units for the pulse to travel from one side of the rod to the other. When the pulse that is resent from PZT0 reaches PZT1 (at 82 time units), then PZT1 begins playing out its pulse. This is where the combination occurs. This combination of waves then travels back towards PZT0.

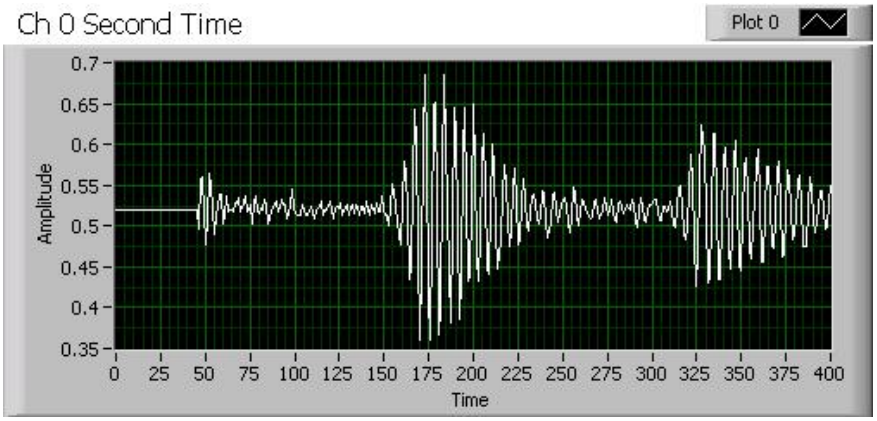

Figure 18. Recording from PZT0 during step 10. The reflected pulse starts to appear at the 164th sample again, except this time it has greater amplitude and appears to be much more defined due to the combination of the reflected pulse and the pulse played out from PZT1.

III. Conclusion

Through experimental results, we have shown that we can perform stress-wave time-reversal in one dimension. Future work will involve the testing of time-reversal in multiple dimensions. Additionally, the time-reversal work will attempt to perform focusing on a crack within a medium. Ongoing work also includes a study of the curing response of epoxy and the way in which acoustic energy affects the response characteristics. Our goal is to put these pieces together in order to demonstrate accelerated self-healing through the use of focused acoustic energy at a damaged point.

Acknowledgements

This work is supported by the Air Force Research Laboratory, Space Vehicles Directorate (AFRL/RV). Particular thanks are due to Mr. Jeremy Banik of AFRL/RV for his insight and continued support. Much gratitude goes to Dr. Robb Winter of South Dakota School of Mines and Technology, Dr. Christopher Jenkins of Montana State University, and the Composite and Polymer Engineering Laboratory (CAPE) of South Dakota School of Mines and Technology. Thanks also go to Mr. Joel Harley, Dr. Jose' M.F. Moura and their team at Carnegie Mellon for their help, input and suggestions.

References

[1]B.L. Lee. Multifunctional design perspective for self-healing and autonomic response. Final Program and Abstract Book 2nd ICSHM - 28 June - 1 July 2009.

[2]S.R. White, N.R. Sottos, P.H. Guebelle, J.S. Moore, M. R. Kessler, S.R. Sriram, E.N. Brown, and S. Viswanathan. Autonomic healing of polymer composites. *Letters to Nature*, 409(15):794–817, February 2001.

[3]X. Sheng, T. C. Mauldin, and M. R. Kessler. Design and synthesis of next-generation monomer healing agents. Final Program and Abstract Book 2nd ICSHM - 28 June - 1 July 2009.

[4]S. Burattini, B. W. Greenland, H. M. Colquhoun, and W. Hayes. A rapidly healable supramolecular polymeric blend. Final Program and Abstract Book 2nd ICSHM - 28 June - 1 July 2009.

[5]W. Nakao and S. Abe. Self-healing rate improvement by shape modification of dispersed silicon carbide particles. Final Program and Abstract Book 2nd ICSHM - 28 June - 1 July 2009.

[6]J. W. Fettig and J. B. Freund. Multi-phase simulation of microvascular self-healing materials. Final Program and Abstract Book 2nd ICSHM - 28 June - 1 July 2009.

[7]V. A. Imperiale and I. P. Bond. A novel self-healing agent able to improve the residual strength of cfrp after impact. Final Program and Abstract Book 2nd ICSHM - 28 June - 1 July 2009.

[8]Chun-Sheng Zhang and Qing-Qing Ni. Bending behavior of shape memory polymer based laminates. *Science Direct - Composite Structures*, 78:153–161, 2007.

[9]W. G. Sloof. Self-healing mechanism in material for high temperature applications. Final Program and Abstract Book 2nd ICSHM - 28 June - 1 July 2009.

[10]G. M. Song, Y. T. Pei, W. G. Sloof, S. B. Li, S. van der Zwaag, and J. Th. M. De Hosson. Oxidation-induced crack healing in Ti_3AlC_2 ceramics. Final Program and Abstract Book 2nd ICSHM - 28 June - 1 July 2009.

[11]A. W. Bosman. Supramolecular materials in motion. Final Program and Abstract Book 2nd ICSHM - 28 June - 1 July 2009.

[12]R. Djugum and R. N. Lumley. Healing and crack closure in an Al-Cu alloy by remedial heat treatment. Final Program and Abstract Book 2nd ICSHM - 28 June - 1 July 2009.

[13]E. B. Murphy, M. L. Auad, and F. Wudl. Stimuli-responsive healable materials: Diels-alder based mending. Final Program and Abstract Book 2nd ICSHM - 28 June - 1 July 2009.

[14]A. Garcia, E. Schlangen, and M. van de Ven. Closing cracks on conductive asphalt mortar by induction heating. Final Program and Abstract Book 2nd ICSHM - 28 June - 1 July 2009.

[15]X. Tang, X. Liang, X. Fan, and Q. Zhou. Syntehsis of ethyl cellulose-based thermal- and photo- dual responsive copolymers via atrp and their aggregates in solution. Final Program and Abstract Book 2nd ICSHM - 28 June - 1 July 2009.

[16]Brian E. Anderson, Michele Griffa, Carne Larmat, Timothy J. Ulrich, and Paul A. Johnson. Time reversal. *Acoustics Today*, 4(1):5–15, January 2008.

[17]Liliana Borcea, George Papanicolaou, and Chrysoula Tsogka. Theory and applications of time reversal and interferometric imaging. *Inverse Problems*, 19:s139–s164, 2003.

[18]M. Fink, D. Cassereau, A. Derode, C. Prada, O. Roux, M. Tanter, J.L. Thomas, and F. Wu. Time reversed acoustics. *Rev. Prog. Phys*, 63, June 2009.

[19]Alexander M. Sutin, James A. TenCate, and Paul A. Johnson. Single-channel time reversal in elastic solids. *J. Acoust. Soc. Am.*, 116(5):2779–2784, November 2004.

[20]Joel Harley, Nicholas ODonoughue, Joe States, Yujie Ying, James Garrett, Yuanwei Jin, Jos M.F. Moura, Irving Oppenheim, and Lucio Soibelman. Focusing of ultrasonic waves in cylindrical shells using time reversal. 7th International Workshop on Structural Health Monitoring 2009.

[21]R.P. Wool and K.M. O'Connor. A theory of crack healing in polymers. *J. Applied Physics*, 52(10):5953–5963, October 1981.